Investigation of the mycobacterial enzyme HsaD as a potential novel target for anti-tubercular agents using a fragment-based drug design approach

Ali Ryan[1], Elena Polycarpou[1], Nathan A. Lack[2,3], Dimitrios Evangelopoulos[4,5,6], Christian Sieg[1], Alice Halman[1], Sanjib Bhakta[4], Olga Eleftheriadou[1], Timothy D. McHugh[5], Sebastian Keany[2], Edward D. Lowe[7], Romain Ballet[2], Areej Abuhammad[8], William R. Jacobs Jr.[9], Alessio Ciulli[10,11] and Edith Sim[1,2]*

[1] Faculty of Science, Engineering and Computing, Kingston University London, Penrhyn Road, Kingston upon Thames, KT1 2EE, UK

[2] Department of Pharmacology, University of Oxford, Mansfield Road, Oxford, OX1 3QT, UK

[3] Present address: School of Medicine, Koç University, Rumelifeneri Yolu, Sariyer, Istanbul, 34450, Turkey

[4] Mycobacteria Research Laboratory, Institute of Structural and Molecular Biology, Department of Biological Sciences, Birkbeck, University of London, Malet Street, London WC1E 7HX, UK

[5] Centre for Clinical Microbiology, University College London, Royal Free Campus, London, NW3 2PF, UK

[6] Present address: Mycobacterial Metabolism and Antibiotic Research Laboratory, The Francis Crick Institute, Mill Hill Laboratory, London NW7 1AA, UK

[7] Department of Biochemistry, University of Oxford, South Parks Road, Oxford, OX1 3QU, UK

[8] School of Pharmacy, University of Jordan, Queen Rania Street, Amman 11942, Jordan

[9] Department of Microbiology and Immunology, Howard Hughes Medical Institute, Albert Einstein College of Medicine, Bronx, New York, 10461, USA.

[10] Department of Chemistry, University of Cambridge, Lensfield Road, Cambridge, CB2 1EW, UK

[11] Present address: Division of Biological Chemistry & Drug Discovery, School of Life Sciences, University of Dundee, James Black Centre, Dow Street, Dundee, DD1 5EH, UK

* Author to whom correspondence should be addressed: email edith.sim@pharm.ox.ac.uk

Abstract

Background and Purpose

With the emergence of extensively drug-resistant tuberculosis there is a need for new anti-tubercular drugs that work through novel mechanisms of action. The *meta* cleavage product hydrolase, HsaD, has been demonstrated to be critical to the survival of *Mycobacterium tuberculosis* in macrophages and is encoded in an operon involved in cholesterol catabolism, which is identical in *M. tuberculosis* and *M. bovis* BCG.

Experimental Approach

We generated a mutant strain of *M. bovis* BCG with a deletion of *hsaD* and tested its growth on cholesterol. Using a fragment based approach, over 1,000 compounds were screened by a combination of differential scanning fluorimetry, NMR spectroscopy and enzymatic assay with pure recombinant HsaD to identify potential inhibitors. We used enzymological and structural studies to investigate derivatives of inhibitors identified and to test their effects on growth of *M. bovis* BCG and *M. tuberculosis*.

Key Results

The *hsaD* deleted strain is unable to grow on cholesterol as sole carbon source but can grow on glucose. Of seven chemically distinct "hits" from the library, two chemical classes of fragments were found to bind in the vicinity of the active site of HsaD by X-ray crystallography. The compounds also inhibited growth of *M. tuberculosis* on cholesterol. The most potent inhibitor of HsaD was found also to be the best inhibitor of mycobacterial growth on cholesterol-supplemented minimal medium.

Conclusions and implications

We propose that HsaD is a novel therapeutic target which should be fully exploited in order to design and discover new anti-tubercular drugs

Ligand	
Cholesterol	Glycerol

Abbreviations: 4,9-DHSA, 4,5-9,10-diseco-3-hydroxy-5,9,17-trioxoandrosta-1(10), 2-diene-4-oic acid; ADC, albumin-dextrose-catalase; BCG, Bacillus Calmette–Guérin; CHES, N-Cyclohexyl-2-aminoethanesulfonic acid; DSF, differential scanning fluorimetry; FBDD, fragment based drug discovery; FCS, fetal calf serum; HOPDA, 2-hydroxy-6-oxo-6-phenylhexa-2,4-dienoic acid; LB, Luria-Bertani; MB, Middlebrook; MCP, *meta*-cleavage product; MDR-TB, multidrug-resistant tuberculosis; MIC, minimum inhibitory concentration; MTT, 3-(4,5-dimethylthiazol-2-yl)-2,5-diphenyltetrazolium bromide; NAT, arylamine N-acetyltransferase; OADC, oleic acid-albumin-dextrose-catalase; PMSF, phenylmethylsulfonyl fluoride; SAR, structure activity relationship; SPOTi, spot culture growth inhibition assay; STD, saturation transfer difference; TB, tuberculosis; TSP, (Trimethylsilyl)-propionic acid; WHO, World Health Organization; XDR-TB, extensively drug-resistant TB.

Introduction

Tuberculosis (TB) remains a global health emergency with an estimated 9 million new cases and 1.5 million deaths every year (WHO, 2015). Importantly, 3.7% of new cases and 20% of previously treated patients are infected with multidrug-resistant tuberculosis (MDR-TB). Moreover, up to 9% of these MDR-TB cases are resistant to nearly all known treatments and considered as extensively drug resistant TB (XDR-TB). Current treatment modalities for drug-sensitive TB cases require continuous dosing for at least 6 months of chemotherapy leading to poor patient compliance, which further increases the rate of drug resistance (WHO, 2015). There is a clear need for new anti-tubercular drugs, particularly those that shorten the treatment period. However, the long-term and indefinite intracellular survival of *Mycobacterium tuberculosis* in different physiological states has made the development of novel therapeutics extremely challenging.

Cholesterol has been identified as important in the infection process of *M. tuberculosis* (Crowe *et al.*, 2015; Lovewell *et al.*, 2016; Ouellet *et al.*, 2011; Peyron *et al.*, 2000) and is used as a carbon source during survival within macrophages (Pandey *et al.*, 2008; Rohde et al., 2012; Van der Geize *et al.*, 2007). In previous work we have demonstrated that an operon consisting of *hsaA* (Rv3567), *hsaB* (Rv3570), *hsaC* (Rv3568), *hsaD* (Rv3569) (Van der Geize *et al.*, 2007) is involved in cholesterol metabolism. This operon was first identified in *M. tuberculosis* and also includes the gene encoding arylamine N-acetyltransferase (*nat,*

Rv3566) (Anderton *et al.*, 2006; Payton *et al.*, 2001) and then further characterized in other mycobacterial species (Evangelopoulos et al., 2014). It is currently believed that the NAT protein may metabolise the alkyl chain generated by cholesterol catabolism (Lack *et al.*, 2009), whilst the other proteins are involved in the degradation of the sterol nucleus of cholesterol (Van der Geize *et al.*, 2007; Griffin *et al.*, 2011; 2012). Studies using transposon mutagenesis have shown that HsaC and HsaD are required for the survival of *M. tuberculosis* within macrophages (Rengarajan *et al.*, 2005). The expression of *hsaC* gene was later demonstrated to be essential both *in vitro* and *in vivo* for infection of *M. tuberculosis* in guinea pigs (Yam *et al.*, 2009). More recent studies have also implicated a role for the operon and HsaD in mycobacterial growth linked to cholesterol catabolism (Griffin et al., 2011). HsaD has also been shown to be overexpressed in hypervirulent strains of *Mycobacterium bovis* BCG during mouse infection (Blanco et al 2009) and compounds with antitubercular activity have been identified as potential HsaD inhibitors via virtual screening (Rebollo-Lopez et al., 2015).

HsaD belongs to the superfamily of αβ-hydrolases that consists of the *meta*-cleavage product (MCP) hydrolase subfamily (Lack *et al.*, 2008). HsaD catalyses the hydrolytic cleavage of carbon-carbon bonds through a serine protease-like catalytic triad (Lack *et al.*, 2008; Lack *et al.*, 2010) of the MCP 4,5-9,10-diseco-3-hydroxy-5,9,17-trioxoandrosta-1(10),2-diene-4-oic acid (4,9-DHSA) in the cholesterol metabolism pathway (Van der Geize *et al.*, 2007). In a previous study, we demonstrated that mechanism-based serine protease inhibitors can inhibit HsaD (Ryan *et al.*, 2014) suggesting that an acyl enzyme intermediate may be formed during the reaction process in line with studies on the mechanism of other C-C bond hydrolases (Ruzzini *et al.*, 2013; Ruzzini *et al.*, 2012). As the HsaC protein (Yam *et al.*, 2009) is unstable in oxygen, HsaD is a promising pharmacological target essential for *M. tuberculosis* infection. It is highly soluble as a stable recombinant protein (Lack et al., 2009) and there are multiple crystal structures available (Lack *et al.*, 2008; Lack *et al.*, 2010). Moreover HsaD has a very large active site cavity that makes it a good target for fragment based drug discovery (FBDD) (Silvestre *et al.*, 2013). FBDD combines NMR, differential scanning fluorimetry (DSF) and crystallography to use weakly binding small molecules (<300Da) as building blocks to develop potent small molecular inhibitors. It is firmly established that fragment screening is a powerful approach to obtain useful start points for inhibitor discovery. Once the biological rationale for a given target is established, then fragment based

approaches are warranted as one of the most effective methods to identify tractable start points for drug design (Ciulli & Abel, 2007; Ciulli, 2013). This approach has shown tremendous success in modern drug discovery (Hudson *et al.*, 2012; Hung *et al.*, 2016) and has been particularly recommended for developing agents against tuberculosis (Marchetti et al., 2016; Mendes & Blundell, 2016).

In this study we investigate HsaD as a novel pharmacological target for tuberculosis through generation of a specific gene deletion mutant and describe the identification of compounds as inhibitors of HsaD by a FBDD approach.

Methods

Bacterial growth conditions

M. tuberculosis, *M. bovis* BCG and *Mycobacterium smegmatis* mc^{2}155 liquid cultures were grown in Middlebrook (MB) 7H9 broth containing 10% (v/v) ADC (albumin-dextrose-catalase), 0.2% (v/v) glycerol and 0.05% (v/v) Tween-80. Mycobacterial strains were also grown on MB7H10 agar containing 10% (v/v) OADC (oleic acid-albumin-dextrose-catalase) and 0.5% (v/v) glycerol. *M. tuberculosis* cultures were grown in 10 mL broth in a 30 mL vials as standing cultures, *M. bovis* BCG in 100 mL broth in a roller bottle rolling cultures at 2 rpm and *M. smegmatis* in 10 mL in a 50 mL centrifuge tubes rotating at 180 rpm all in a 37°C incubator, unless specified otherwise. Δ*hsaD M. bovis* BCG was further supplemented with 50 μg/mL hygromycin.

Growth curve comparison of the wild-type and Δ*hsaD M. bovis* BCG were done in minimal medium containing 0.05% (v/v) tyloxapol and 0.05% (v/v) ethanol with either a) no additional carbon source, b) 100 μg/mL glycerol or, c) 100 µg/mL cholesterol. An equivalent number of bacteria (6 x 10^8) were added to start the cultures and the bacterial growth rate was measured by monitoring the OD$_{600}$ daily for 16 days.

E. coli JM109 cells were grown in Luria-Bertani (LB) broth 10 mL of a centrifuge tube rotating at 180 rpm a 37°C incubator. LB agar was used for solid growth of *E.coli* strains at 37°C, unless specified otherwise.

Generation of the Δ*hsaD* gene deletion

Deletion of the *hsaD* gene was performed using specialised transduction as previously described (Bardarov *et al.*, 2002). Briefly, the upstream and downstream flanking DNA regions of the *hsaD* gene were amplified by PCR using the following pair of oligonucleotide primers for the upstream flanking DNA region 5'-TTTTTTTTGCATAAATTGCAGGCACCGTAGGCCAT-3' and 5'-TTTTTTTTGCATTTCTTGCAGTGACGTCCATTCAACA-3' as the forward and reverse primers respectively with a *Bst*API restriction site (underlined). The primers for the downstream flanking region were 5'-TTTTTTTTCACAGAGTGCTTGACCGAGGCAATTGGAGAC-3' and 5'-TTTTTTTTCACCTTGTGCACCTGTTGGGCGGGC-3' as the forward right and reverse primers respectively with a *Dra*III restriction site (underlined). The upstream and downstream products were subsequently digested with *Dra*III and *Bst*API, respectively, and ligated with *Pfl*MI-digested p0004s vector arms. The knockout construct was linearised following digestion with *Pac*I and cloned into phAE159. Both pAES and phAE159 were subsequently digested with *Pac*I, gel purified and ligated with T4 DNA ligase. The ligation mixture was then packaged into λ phage heads by *in vitro* packaging, transduced into *E. coli* and plated on LB agar supplemented with hygromycin. Following validation the phasmids were then electroporated into *M. smegmatis* and grown at a permissive temperature (30°C) to generate mycobacteriophages. The resulting high-titre mycobacteriophages were then used to transduce the recipient mycobacteria at 37°C (non-permissive temperature). The correct identity of loss-of-function mutations was confirmed by PCR amplifications with primers against the internal *hsaD* gene (forward: 5' AAGTCGGCTCCGGC 3' reverse: 5' TGGCCGTCGACCAGC 3') and the region flanking the *hsaD* deletion (forward: 5' GATGCTCATCTGCCACC 3' reverse: 5' ATGACAGCTACCGAGGAAT 3').

Intracellular survival of Δ*hsaD M. bovis* BCG in macrophages

The RAW264.7 mouse macrophage cells were grown as a monolayer in RPMI-1640 media (GIBCO, Paisley, UK), supplemented with 1% (w/v) L-glutamine and 10% (v/v) foetal calf serum (FCS) at 37°C with 5% CO_2. For the intracellular survival assays, RAW264.7 cells

were plated approximately 24 hours prior to infection on 6-well plates in the presence of 2 mL RPMI (supplemented with 10% (v/v) FCS) as described (Bhakta et al., 2004; Westwood et al., 2010). Cells were subsequently washed with fresh media, infected with *M. bovis* BCG at a multiplicity of infection of 20 (i.e for every 1 RAW264.7 cell, 20 cells of *M. bovis* BCG were added) and incubated for 2 h. Cells were then washed twice with PBS and re-suspended in fresh medium. The medium was later removed and the cells were lysed with 1 mL of sterile distilled water for 10 min at 0, 24, 48, 72 and 120 h. The number of intracellular bacteria was determined by serially diluting the lysate, plating it on MB7H10 agar plates and incubating at 37°C for 3-4 weeks.

Effect of inhibitors against *M. tuberculosis* grown in cholesterol

The minimum inhibitory concentrations (MIC) of selected inhibitors, were determined using the spot culture growth inhibition assay (SPOTi). This method has been compared favourably with other methods of MIC determination (Evangelopoulos & Bhakta, 2010). Briefly, mycobacteria were plated in 24 well plates on minimal agar based media containing: asparagine (0.5 g/L), KH_2PO_4 (1.0 g/L), Na_2HPO_4 (2.5 g/L), ferric ammonium citrate (50 mg/L), $MgSO_4,7H_2O$ (0.5 g/L), $CaCl_2$ (0.5 mg/L), $ZnSO_4$ (0.1 mg/L), agar (1.5% w/v) and either glycerol (0.1% v/v) or cholesterol (0.01% w/v). Fragments dissolved in DMSO (0.0125 μg/mL, 0.025 μg/mL, 0.05 μg/mL, 0.1 μg/mL, and 0.2 μg/mL) or DMSO alone were mixed with 2 mL of the minimal media with cholesterol per well. The final DMSO concentration in the wells containing fragments was 0.2%. In addition a well with 0.2% DMSO only as well as isoniazid at various concentrations (0.001 μg/mL, 0.01 μg/mL, 0.1 μg/mL, 1 μg/mL and 10 μg/mL) were used as positive controls. The inhibitors and isoniazid were prepared by one experimentalist and supplied as a numbered array such that growth experiments were carried out blinded.   The plates were then inoculated with 2 μL (approximately 10^3 viable cells) of a mid-log phase culture of either *M. bovis* BCG or *M. tuberculosis* that was added in the centre of each well and allowed to soak before the plates were sealed with para-film, wrapped with aluminium foil and incubated at 37°C for 2 weeks until a spot of colonies were developed in the control wells. The MIC was determined as the lowest concentration in wells where mycobacterial growth was not evident. This was repeated in triplicate in three independent experiments and the same MIC values were obtained in all experiments.

Effect of inhibitors against *E. coli*

An overnight culture of *E. coli* JM109 cells grown as stated before was diluted in LB media to a final OD_{600} of 0.1 and acted as a working culture. 10μL of this working culture was used to inoculate a 96 well plate containing 90μL of LB media with a range of inhibitor concentrations up to 100 μg/mL. The maximum DMSO concentration in the well was 1.7% (v/v). The plates were then transferred into the Tecan M200 Infinite Pro spectrophotometer where they grew at 37°C as standing cultures with absorbance measurements at 600nm taken every hour for 4 hours

Cytotoxicity against mammalian cells

Cytotoxicity was tested using CCL-228 colorectal cancer cells (American Tissue Culture Collection Manassas, VA). Cells were cultured in Dulbecco's Minimum Essential Medium (GIBCO, UK), supplemented with 10% (v/v) foetal bovine serum (FBS; Sigma-Aldrich, Poole, UK), 10,000U penicillin, 10 mg/mL streptomycin in 0.9% NaCl (Sigma-Aldrich), and maintained at 37°C in a humidified atmosphere with 5% CO_2. Cells were seeded in 96-well plates (20,000 cells/well) and treated for 48 h after which they were incubated with 100μL of 50μg/mL MTT solution in phenol red free DMEM (GIBCO) for 3 h in the dark at 37°C. The MTT was removed and the crystals solubilised with 100μL DMSO for 15 min at room temperature with gentle shaking. The intensity was measured colorimetrically at 570 nm using the M200 Infinite Pro plate reader (Tecan) and percent growth was calculated. Thesestudies were carried out blind by one experimenter (EP) using numbered samples provided by AR with the numbers randomised in 5 separate experiments.

Fragment based drug discovery

Differential scanning fluorimetry (DSF) was performed on a total of 1258 fragments as described previously (Niesen *et al.*, 2007), using 0.4-1 μM HsaD in the presence of 2.5× SYPRO orange (Invitrogen) and 2.5 mM of compound (0.5 μL from a 0.1 M stock) at a final volume of 100 μL per well (final dmso concentration of 2.5%) in 50 mM HEPES 300 mM NaCl pH 7.5. Fluorescence was monitored using an Agilent Mx3005p qPCR instrument (Santa Clara, USA). The fluorescence excitation and emission wavelengths were 483 and 533 nm. The output data was plotted as derivative of the fluorescence versus temperature, and the maximum of such derivative over temperature was determined as the melting temperature (T_M). The primary DSF screen was carried out three times in triplicate and the repeat screen was also carried out three times in triplicate making a total of six independent determinations in triplicate for each compound identified as a hit. Hits were identified by the shift in T_M

compared to HsaD with vehicle according to previously described methodologies (Cuilli, 2013.

NMR fragment screening

Confirmed hits were validated by ligand-observed NMR spectroscopy (Ciulli *et al.*, 2007; Dalvit *et al.*, 2001; Ferguson *et al.*, 2013). All NMR experiments were carried out at 278 K on a Bruker Avance 700 MHz equipped with a 5 mm triple TXI cryoprobe with *z* gradients. Relaxation-edited NMR experiments incorporated a CPMG spin-lock time of 200 ms before the acquisition period (Carr & Purcell, 1954). . Saturation Transfer Difference (STD) NMR experiments employed a 40 ms selective Gaussian 180° shaped pulse at a frequency alternating between 'on resonance' (0.5 ppm) and 'off resonance' (~80 ppm) after every scan (Mayer & Meyer, 1999). Water suppression was achieved by using a W5 Watergate gradient spin-echo pulse sequence (Piotto et al., 1992). WaterLOGSY experiments (Dalvit *et al.*, 2000; 2001) employed a 20 ms selective Gaussian 180° shaped pulse at the water frequency and an NOE mixing time of 1 s. Water suppression was achieved using a double-gradient echo excitation sculpting sequence with gradients. The resulting spectra were analyzed using Topspin 2.0 software (Bruker). All samples were made up to a total volume of 200 µL in 3 mm capillaries, and contained 1.2 mM fragment, 50 mM Tris-HCl buffer at pH 7.5, 10% v/v D_2O, and 2.4% v/v DMSO-d_6. (Trimethylsilyl)-propionic acid-d_4 (TSP) was present at 20 µM concentration in all samples for calibration purposes. A protein only control sample was run as buffer control. Each fragment was run as 3 samples – (A-C). A) Fragment only; B) Fragment + protein (10 µM HsaD); C) Fragment +HsaD + displacer compound PMSF (100 µM).

Enzymatic assays

Following the initial identification of fragments from the fragment based drug design library, inhibition assays were carried out as previously described (Ryan et al., 2014) in the presence of 1 mM with compounds **1-7**. Subsequently, compounds that were capable of inhibiting the cleavage of HOPDA by HsaD, were further selected for IC_{50} determination using a range of concentrations (1 mM, 0.5 mM, 0.375 mM, 0.25 mM, 0.125 mM, 0.05 mM and 0 mM or 3.5 mM, 3 mM, 2.5 mM, 2 mM, 1.5 mM, 1 mM, 0.5 mM and 0 mM). Briefly pure HsaD (16 µg/mL in 100 mM phosphate buffer pH 7.5, 20 mM NaCl) was added to the reaction mixture

in the presence of 100 μM HOPDA (final concentration of 1% ethanol v/v) and inhibitor (final DMSO concentration of 5%) in a final volume of 100 μL. The enzymatic activity was measured by monitoring the absorbance at 450 nm at 21°C using a M200 Infinite Pro plate reader (Tecan) and the IC_{50} was determined using GraphPad Prism. The ε_{450} of HOPDA was measured as 13,200 $M^{-1}cm^{-1}$. N values refer to the number of independent experiments.

Solution of the structures of HsaD with Fragments 2, 27 and 32

Crystals of apo-HsaD were grown as described previously (Lack *et al.*, 2008). All fragments were dissolved directly into the cryoprotectant containing 30% (w/v) PEG-3000, 0.1 M CHES pH 9.5, 25% (v/v) glycerol, at concentrations of between 15 mM and 50 mM. Crystals were transferred into the cryoprotectant containing one of the fragments and allowed to soak overnight at 21°C before flash freezing for analysis.

Data collection for the structures of HsaD bound to **2**, **27** and **32** were all performed at the Diamond Light source (Oxon, UK) using beamline I24 in the case of the structure with **2** and using beamline I03 for the others. In all cases initial processing was performed via Xia2 (Winter, 2010) using XDS (Kabsch, 2010) to index and either Scala (**2**) (Evans, 2006) or Aimless (Collaborative Computational Project, 1994; Winn *et al.*, 2011) (**27** and **32**), to merge and scale the data. The structure was solved via molecular replacement using PHASER (McCoy *et al.*, 2007) using the structure of apo-HsaD (PDB code, 2vf2) (Lack *et al.*, 2008) stripped of all ligands as a search model. The atomic models were rebuilt in COOT (Emsley *et al.*, 2010) and refined using REFMAC (Murshudov *et al.*, 1997) and PHENIX (Adams *et al.*, 2010). Model restraints for **2**, **27** and **32** were generated in eLBOW (Moriarty *et al.*, 2009).

Data and Statistical analysis

The data and statistical analysis comply with the recommendations on experimental design and analysis in pharmacology (Curtis et al., 2015). Samples were randomised in all 96 well experiments and sample identity was not known to the investigator. Data is shown as the mean plus or minus the standard deviation and IC_{50} values in enzymic inhibition assays were determined via non-linear fit analysis in Graphpad Prism.

Software tools to fit raw data obtained from differential scanning fluorimetry for data visualization and analysis were used based on Microsoft Excel and were obtained from the Structural Genomics Consortium Oxford (ftp://ftp.sgc.ox.ac.uk/pub/biophysics), see also (Niesen et al 2007). The entire fluorescence raw data (RFU) from the thermal melt curve was accurately fitted to a Maxwell-Boltzman distribution in Graphpad Prism.

Materials

All reagents were purchased from Sigma Aldrich (Poole, UK) unless otherwise stated. 3,5-dichlorobenzenesulphonamide, 3-chloro-4-hydroxybenzoate, 4-toluenesulphonamide and 2-oxovaleric acid were obtained from TCI Europe. 3,5-diflurobenzenesulphonamide, 3,5-dichlorobenzamide and 3-bromobenzenesulphonamide were obtained from Apollo Scientific and ethyl-3,5–dichloro-4-hydroxybenzoate was obtained from Maybridge. The fragment library used in this study was composed of 1258 compounds from commercial libraries supplied by Maybridge (Thermo Fisher Scientific: http://www.maybridge.com/), as previously described (Ciulli, 2013; Van Molle *et al.*, 2012). All library compounds were dissolved and stored in d_6-DMSO.

All inhibitors were dissolved in DMSO. The DMSO final concentration in the assays was 5% (v/v) for the enzymatic assays and between 0.02% and 1.7% (v/v) for the growth experiments. The synthetic substrate, 2-hydroxy-6-oxo-6-phenylhexa-2,4-dienoic acid (HOPDA) was synthesised by Almac Sciences (Craigavon, Northern Ireland) as previously described and dissolved in ethanol (1% v/v) (Lack et al., 2009). The fragment library was prepared as previously described (Ciulli, 2013; Van Molle *et al.*, 2012).

Results

Growth

Deletion of *hsaD* in *M. bovis* BCG ($\Delta hsaD$) was generated using a mycobacteriophage-based knockout method (Bardarov *et al.*, 2002). All of the hygromycin resistant colonies tested were the correct mutant. Our results are in accordance with previous studies, which have

reported that approximately 95% of antibiotic-resistant transductants were the correct genotype (Bardarov *et al.*, 2002).

When grown in MB7H9 broth (Figure 1A) or in minimal medium (Figure 1B) the deletion of *hsaD* had no apparent effect on bacterial growth when compared with *M. bovis* BCG. However, when the minimal medium was supplemented with cholesterol (Figure 1C), a significant difference between the two strains was observed. Whilst the growth of the wild type strain was very similar to that in minimal medium alone, the growth of *ΔhsaD M. bovis* BCG was significantly inhibited in the presence of cholesterol as compared to *M. bovis* BCG (Figures 1B & C). The growth of *ΔhsaD M. bovis* BCG in the presence of cholesterol was suppressed compared with growth in minimal medium alone.

Growth in minimal medium with glycerol as the sole carbon source is supported in both the *ΔhsaD* strain and *M bovis* BCG. The gene deleted strain showed a slight lag in rate of growth although it caught up by day 16, reaching the same optical density ($OD_{600} = 1.5$) (Figure 1D).

The intracellular survival of the wildtype and *ΔhsaD* strains of *M. bovis* BCG within RAW246.7 shows that, similar to *ΔhsaC* and *Δnat* strains, there was a reduction in intracellular growth of the *ΔhsaD* strain as compared to *M. bovis* BCG (Figure 1E).

We also deleted *hsaD* from *M. smegmatis* and when it was grown on cholesterol as carbon source the culture turned pink .(Supplementary Figure 1) .

Identification of chemical fragments as inhibitors of HsaD

A commercial library of rule-of-three compliant 1258 fragments (Silvestre *et al.*, 2013) was screened by DSF. The melting temperature of pure recombinant HsaD was monitored in the presence of the fragments. The melting temperature of HsaD in previous studies (Lack *et al.*, 2009) had been determined by circular dichroism and loss of enzymatic activity of the protein itself to be between 69 and 72°C. The high melting temperature was confirmed by DSF monitored by SYPRO Orange to be 72.7 (average mean value from quadruplicates across 17 plates) +/- 0.21°C (average SD from quadruplicates across 17 plates) in the presence of solvent and no added fragment. Fragments were identified as potential binders to purified HsaD when a shift was monitored in the melting temperature of greater than two standard deviations from the mean melting temperature of pure HsaD alone (Table 1). Hit compounds (18) from the primary screen were re-tested in duplicates in the thermal shift assay, from which 8 were confirmed. The validated fragments were also tested as inhibitors of HsaD at a

concentration of 1 mM of the compound (Figure 2) and were in addition tested by saturation transfer NMR for displacement by PMSF, an already identified inhibitor (Ryan *et al.*, 2014) (Table 1 & Figure 2A).

From this combination of methods, a series of seven distinct fragments were identified as binders. Fragment 1 was not pursued further due to its insolubility at 1 mM. In addition to the "hits" from the screen, a selection of 20 compounds from the library which showed no evidence of binding by the DSF criteria, were also tested at 1 mM as inhibitors of HsaD and none were found to inhibit the enzyme (Data not shown) . From the initial inhibition studies at 1 mM, two compounds looked promising - compound **2** and compound **6**, which produced 38 % and 60% inhibition respectively (Figure 2). Fragment **2** is a sulphonamide and fragment **6** is a hydroxybenzoate.

When tested at a range of concentrations, compound **2** (3,5-dichlorobenzenesulfonamide) is an inhibitor of HsaD with an IC_{50} of 0.41 mM (Table 2) and fragment **6** (ethyl 3,5-dichloro-4-hydroxybenzoate), despite it not being displaced by PMSF (Table 1) , is also an inhibitor of HsaD with an IC_{50} of 0.52 mM (Table 2).

The fragments which were identified were distinct from previously identified substrates (Lack *et al*., 2010) and also distinct from putative inhibitors identified from a virtual screen (Rebollo-Lopez *et al*., 2015) but interestingly bear some resemblance to the central moiety of an inhibitor identified as targeting the HsaAB protein complex of the same operon (Vanderven *et al,* 2015).

A small series of compounds related to each of the two classes of hit fragments 2 and 6 was tested for inhibition of HsaD (Supplementary table 1).

Derivatives of fragment 2 as inhibitors of HsaD

We investigated the small series of fragments modified around Compound **2** which has two chlorine atoms at the *meta* position. We investigated the effects of altering the position and number of chlorines in the molecule as well as substituting different halide groups. Removal of one chlorine from position 3 (Compound **9**) was detrimental to the inhibitory potency and the IC_{50} was increased more than 10 fold to 5 mM (Supplementary table 1). Removal of both the chlorine atoms as in compound **8** (Table 1 supplementary & Table 2), destroyed inhibition of HsaD completely. Substitution of the chlorines by fluorine (Fragment **10**) also resulted in loss of inhibition of HsaD (Table 1 Supplementary).Having a single chlorine in

the *para* position (Fragment **13**) did not possess any inhibitory effects on HsaD (Supplementary Table 1).

Altering the position of chlorine from *meta* to the *ortho* position (Fragment **11**) likewise resulted in a decreased inhibitory effect (IC$_{50}$ 1.89 mM) compared with fragment **2** and changing the chlorines to trifluoromethyl compounds (fragment **12**) showed poorer inhibition as compared to the initial compound with less than 50% inhibition being reached. (Supplementary Table 1). Mono-substituted benzenesulfonamides with a bromine in position 3 (Fragment **14**), like the mono-chlorinated fragment, produced a similar IC$_{50}$ of 2.69 mM.

The library of fragments used for these studies also incorporated sulphonamide fragments with the addition of nitro-, amino-, methyl-, methoxy-, hydroxy-, and carboxy- groups on various positions of the benzene ring. None of the modifications including these side groups were capable of inhibiting HsaD (Fragments **15-23**) with the exception of Fragment **20** which, with an IC$_{50}$ of 92.6 mM, was an extremely poor inhibitor.

A derivative of Fragment **2**, 3,5-dichlorosulfanilamide in which an amide group was incorporated in position 4 of the benzene ring, was able to inhibit HsaD with an IC$_{50}$ of 0.16 mM (Fragment **24**) (Table 2 and Supplementary Table 1). Addition of a dimethyl group on the nitrogen (Fragment **25**), however reduced the inhibitory effect on HsaD with an IC$_{50}$ of 3.68 mM. Replacement of the chlorines with bromines (Fragment **26**) reduced the inhibitory potency compared with the parent compound to IC$_{50}$ 2.10 mM.

The important features for inhibition of HsaD by derivatives of **2** appear to be a *para* hydroxyl group on the aromatic ring and two chlorines as *meta* substituents and the inhibitory potency (IC50 of 0.27mM) of fragment 27 supports this conclusion. Fragment 27 also has a sulfonate group at position 1 (Table 2).

Derivatives of compound 6 as inhibitors of HsaD

A small group of hydroxybenzoate analogues were tested for comparison with compound **6** as inhibitors of HsaD.

Like compound **2**, compound **6** has *meta* (3,5) substituted chlorine atoms and the position and number of chlorine substituents on the aromatic ring was altered as well as the presence of the 4-hydroxyl group.

Ethyl 3,5-dichloro-4-hydroxybenzoate (Fragment **6**) inhibited HsaD (IC$_{50}$ 0.52 mM). When the hydroxyl group was removed there was no inhibition of HsaD (Fragment **28**) and when either one or both of the chlorine atoms were removed no inhibition was then observed. Fragment **29** with only one chlorine at the 3 position was not inhibitory and the same was true when both chlorines were missing (Compound **30**).

An analogue in which both the chlorines are present and the 4 hydroxyl is present but there is a change in the ester substituent on the 1 position to a carboxylate group (3,5-dichloro-4-hydroxybenzoic acid - Fragment **32**) has the same IC$_{50}$ value of 0.54 mM as the parent compound (Table 2B and Supplementary table 1). If the hydroxyl group in this charged compound is substituted by an amino group (fragment **33**), the IC$_{50}$ remains essentially the same (0.55 mM). Interestingly, altering the ethyl substituent on the carboxylate group to a methyl group (compound **31**) was inhibitory but with a slightly higher IC$_{50}$ (0.71 mM).

To further elucidate the importance of the chlorines on positions 3 and 5, these were rearranged into positions 1 and 3 with the addition of a nitro group in position 6 (Fragment **35**). The resulting compound was less inhibitory, with an IC$_{50}$ of 2.15 mM. Removal of the chlorines and only the presence of the carboxylic acid and amine group in positions 1 and 4 of the benzene ring respectively (Fragment **36**) and the amine in position 3 (Fragment **37**), completely reversed the inhibitory effect (supplementary Table 1).

Structural studies of HsaD with inhibitors

In order to identify the mode of binding of the inhibitors which were identified, structural studies were carried out using three different inhibitors : Compound **2** (IC$_{50}$, 0.52mM) and an analogue (compound **27**, IC$_{50}$, 0.27mM) were chosen as representatives of the sulphonamide series and compound **32** (IC$_{50}$, 0.54mM) was chosen as a representative of the hydroxybenzoate class. The latter compound was chosen in preference to the parent compound because it is more soluble. Crystals of HsaD were soaked with the inhibitory fragments.

The crystal structure of HsaD with compound 2, was obtained to a resolution of 2.1 Å. The crystal structure with 3,5-dichloro-4-hydroxybenzenesulphonic acid (fragment 27) was obtained at a resolution of 2.68 Å and the structure of HsaD was also obtained where the ligand bound was a derivative of hydroxybenzoic acid (3,5-dichloro-4-hydroxybenzoic acid

Fragment 32), at a resolution of 2.27 Å. Processing and refinement statistics for all three structures are shown in table 3.

The crystal structures of each of these ligand bound structures can be compared with the structure of HsaD alone (Figure 3A). With the exception of a 55° rotation of the side chain of Trp270, which is only observed in the structure of HsaD with compound 2, there are no major conformational changes compared with structure of apo-HsaD (overall RMSD 0.2 - Figure 3). The binding of substrate molecules to HsaD revealed the presence of two different conformations, an open conformation for the apo-enzyme and a closed conformation when the substrate was bound. However, there was no change in the juxtaposition of the active site residues in the main catalytic pocket. The same is true on the binding of the inhibitors which have been investigated here (Figure 3A).

Two molecules of fragments 2 and 27 were observed bound to HsaD, in their respective structures: one molecule was bound in each of the active sites of the protomers in the dimer in the asymmetric unit. In each of these cases the orientation of the ligand was superimposable with its orientation in each of the two active sites in the dimer.

Compound 32 was found in only one of the active sites of the dimer in the asymmetric unit, with the A chain active site being unoccupied. This reflects the data obtained with the substrate bound structures (Lack *et al.*, 2010). The inhibitor binding sites each overlap with the binding site of the substrate from previous structures (Figure 4D) and are close to the active site Ser (Fig 3B-D). These structural studies confirm the specificity of the screening process in identifying inhibitors of HsaD.

Binding of 2 and its analogue 27 to HsaD

The structure of HsaD bound to fragment **2** allowed the unambiguous determination of the fragment's binding orientation. Fragment **2** binds within the active site with its sulphonamide group making short-range hydrogen bonds with the side chain of Asn244 (Figure 3B). It also forms a hydrogen bond with the backbone amide of Gly140 and a water bridged interaction with the side chain of Asn89. The benzene ring forms hydrophobic contacts with Gly46 and the side chains of Leu115, Leu158 and Val243. One chlorine forms contacts with the side chains of Met208 and Phe220, while the other contacts the side chains of Phe173 and His269.

The number of hydrophobic contacts made by the chlorines explains why removal of one or both has a detrimental effect on fragment binding (Fragments **8** and **9**) and also why

replacement of the chlorines with polar functional groups is energetically unfavourable Fragments (**16**, **18**, **20**). The importance of the interactions of chlorines at positions 3 and 5 also explains the inability of **17**, **21** and **22** to inhibit HsaD. The hydrophobic contacts with Met208 and Phe220 are relatively long range (4.3 Å and 4.8 Å respectively) which indicates why the bromine of the inhibitory fragment **14** could be accommodated.

The short-range hydrogen bond formed by the sulphonamide nitrogen explains the detrimental effect observed by double methylation of this group in fragment **25**. Accommodation of the sulphanilamide of **24** in the current orientation would not be possible due to the distance between the fragment's ring and Gly46 being too short to allow accommodation of an amine group in between (3.7 Å).

Fragment **27** binds with its acidic group at the entrance of the polar sub-pocket (Fig 3C) that binds the dienoate moieties of HOPDA and 4,9-DHSA (Lack *et al.*, 2010). The sulphonate group of **27** forms hydrogen bonds with the side chain of Trp270 as well as the backbone amides of Gly45 and Gly46 (Figure 3C). The sulphonate also forms a salt bridge interaction with the side chain of Arg192 (4.5 Å). One of the chlorines of **27** fits into a hydrophobic pocket formed by the side chains of Leu158, Phe173, Met177 and Val243 (all distances <4Å). The other chlorine interacts with Gly45 and the side chain of Leu115.

The acidic compound **27**, binds in a different orientation to the uncharged sulphonamide **2** (Figure 4B). The charged sulphonate group of **27** may drive its binding to the polar pocket of the active site where it is able to form the salt bridge with Arg192 that could not be formed with the neutral sulphonamide of **2**. This clear distinction in the binding modes of fragments that have charged versus simply polar groups provides useful information for modifying the fragments to improve affinity.

Binding of fragment 32 to HsaD

Fragment **32** binds in an almost coplanar conformation to **27** (Figure 3D)**.** However, its binding position is shifted by around 1.8 Å outward from the polar sub-site (Figure 4). As a result, the carboxyl group of **32** is not inserted as far into the pocket as the sulphonate of **27**. The carboxyl group forms hydrogen bonds with the side chain of Ser114 and the backbone amides of Gly45 and Gly46 (Figure 3D). This also means the fragment is unlikely to form a salt bridge with Arg192 (separation >6 Å). The altered binding conformation also removes the interaction of the chlorine with Gly45, leaving only the contact with Leu115. The other

chlorine still contacts Leu158, Phe173 and Val243 but does not contact Met177, rather, it interacts with Val155.

The extensive hydrophobic contacts made by both chlorines of **32,** explains their importance in the binding of the fragment. In view of the proposed importance for the 4-hydroxy group of **32** in the inhibition of HsaD, it was unexpected to find the hydroxyl group makes no interactions with either the side chain or backbone of HsaD.

The binding of **32 (Figure 3D)**, like the other acidic inhibitor investigated (**27 Figure 3C**) shows a distinct binding orientation from the uncharged sulphonamide (fragment 2) Figure 3B.

From these comparisons of binding sites, using fragment **2** as a starting point (Figure 4) there are two possible areas of expansion, the first is into the polar pocket that is accessed by the acidic groups of **27** and **32** (Figure 4C). The second area of expansion would be into the strongly negatively pocket in close proximity to the sulphonamide group of **2**. Expansion into this polar pocket would mimic that of HOPDA (Figure 4D) which extends deep into the pocket and makes shorter range salt bridge with Arg192 (3.1 Å).

Effects of inhibitors on growth of *M. bovis* BCG and *M. tuberculosis* H37Rv.

In order to evaluate the specific anti-mycobacterial activity of the compounds, we tested them for inhibition of growth of *E. coli.* There was no inhibition observed at up to 100 μg/mL (Supplementary Figure 2). We also tested for any cytotoxic effect against RAW264.7 murine macrophage cells and again found no evidence of eukaryotic cell toxicity at concentrations up to 100 μg/mL (data not shown).

None of the HsaD inhibitors had any effect on the growth of *M. bovis* BCG or *M. tuberculosis* when cultured in enriched MB7H9 broth. This observation is consistent with the effect seen in the gene deleted mutant strains. In order to test the proof of principle that inhibitors of HsaD would have an effect on the growth of *M bovis* BCG and *M. tuberculosis* on cholesterol, we tested the fragments at concentrations ranging from 12.5 μg/mL to 200 μg/mL in minimal growth media supplemented with cholesterol, using the SPOTi assay. Fragment **6** which is one of the most potent inhibitors of HsaD was also the most effective at

inhibiting growth of both *M. bovis* BCG and *M. tuberculosis* in the presence of cholesterol, with growth only at 12.5 µg/mL. On the other hand, fragment **8** which showed no inhibition of HsaD was also ineffective at concentrations up to 200 µg/mL in inhibiting the growth of either *M. bovis* BCG or *M. tuberculosis* on cholesterol.

Fragment **2** was capable of inhibiting the growth of *M. bovis* BCG cells with an MIC of <12.5 µg/mL whilst fragment **24**, inhibit the growth at 25 µg/ml. Fragment **27** on the other hand, did not appear to have an effect, with growth evident even at the highest concentration (200 µg/mL). As with fragment **2**, both fragments **6** and **32**, completely halted growth, with an MIC below 12.5 µg/mL. Isoniazid, gave an MIC of 0.1 mg/mL on bacteria grown on cholesterol.

Similarly, the effect on *M. tuberculosis* growth following treatment with the fragments was also investigated during growth on cholesterol. Treatment with fragments **2** and **6** gave an MIC of 50 µg/mL and 25 µg/mL respectively, whilst fragments **24** and **32**, 200µg/mL. No inhibition was observed with fragments **27** and **8** (growth present at 200 µg/mL) therefore, the MIC could not be calculated. Isoniazid was again found to have an MIC of 0.1 mg/mL. Fragment 27 is negatively charged and is ineffective in the inhibition of growth (see discussion below).

Discussion and Conclusions

We have investigated the role of *hsaD* in mycobacteria and determined whether the gene product is a suitable target for developing anti-tuberculars using a fragment based approach to identifying inhibitors of the HsaD enzyme. We have confirmed effects on growth of deleting the *hsaD* gene and used structural studies to demonstrate the binding of inhibitors identified by this method. We have also demonstrated that inhibitors of the enzyme inhibit the growth of *M. tuberculosis* on cholesterol.

Role of HsaD in growth

There is growing evidence from whole genome studies of the importance of cholesterol for intracellular survival of *M. tuberculosis* and recurring evidence for the importance of the operon encoding HsaD as being essential for intracellular survival of *M. tuberculosis* and *M. bovis* BCG. We show here that this is the case in studies where we have created a targeted

deletion of *hsaD* from *M. bovis* BCG. We demonstrate that the growth of *ΔhsaD M. bovis* BCG on miminmal medium plus cholesterol is inhibited (Fig. 1C).

In addition to the effects on the growth pattern of the *ΔhsaD M. bovis* BCG strain on cholesterol, we also generated a *ΔhsaD* strain of *M. smegmatis* and we observed a pink colour when the latter strain was grown on minimal medium plus cholesterol in liquid culture (supplementary Fig. 1.) The same observation has been made when a *ΔhsaC M. tuberculosis* H37Rv strain is grown in minimal medium with cholesterol (Yam *et al.*, 2009). Therefore, similar to the "pink" metabolite of the *ΔhsaC M. tuberculosis* we propose that deletion of *hsaD* results in inhibition of growth of *M. bovis* BCG on cholesterol as a result of accumulation of an inhibitory metabolite.

In addition to effects on growth on cholesterol, we have also noted a lag in growth on glycerol in minimal medium of the Δ*hsaD* strain (Fig. 1D). This mirrors previous findings on deletion of *hsaD* and other essential genes involved in cholesterol catabolism from *M. tuberculosis* (Griffin et al., 2011). Additionally it has been observed that *hsaD* expression is significantly increased in *M. smegmatis* when grown on cholesterol (Uhía *et al.*, 2012) and genome wide studies with *M. smegmatis* grown on cholesterol have also pointed to an increase in HsaD expression on growth on cholesterol (Li et al., 2016).

We have also investigated growth in macrophages. Whole genome studies have previously identified the role of HsaD in the survival of *M. tuberculosis* within macrophages (Sassetti *et al.*, 2003). It has also been demonstrated that other genes in the operon (*hsaC* and *nat*) are essential for survival of *M. bovis* BCG in macrophage (Anderton *et al.*, 2006; Bhakta *et al.*, 2004).

Similar to Δ*hsaC* and Δ*nat* strains, there was a reduction in intracellular growth of the Δ*hsaD* strain as compared to the *M. bovis* BCG (Fig. 1E). This is consistent with the whole genome studies and studies identifying the role of other members of this operon in the metabolism of cholesterol, which has been identified as controlled as the *Kst*-Regulon (Kendall et al., 2007; Kendall *et al.*, 2007; Uhia *et al.*, 2012)).

Identification of chemical fragments as inhibitors of HsaD

The studies described above add to the growing weight of evidence that the operon in which *hsaD* is encoded along with the *nat* gene in the same gene cluster (Anderton *et al.*, 2006) are

essential for intracellular survival of mycobacteria and also that the gene product are required for cholesterol metabolism in *M. bovis* BCG and *M. tuberculosis* (Kendall *et al.*, 2010; Van der Geize *et al.*, 2007; Yam *et al.*, 2009). Given this importance, we speculated that the *hsaD* gene is a potential target for anti-tubercular agents. Supporting drug design, the crystal structure of HsaD has been established to better than 2 Å resolution with the substrate HOPDA bound and shows that the active site cleft is over 2100 $Å^3$, which is a good prospect for a fragment based approach to identifying inhibitors (Lack *et al.*, 2008). HsaD is also a stable soluble protein which crystallises readily (Ryan *et al.*, 2014). Moreover, chemical inhibitors of HsaAB were found to dramatically decrease the intracellular proliferation of *M. tuberculosis* in macrophages (VanderVen *et al.*, 2015).

Fragment based drug discovery relies on having crystallographic data. The structure of HsaD has been determined alone (Lack *et al.*, 2008) to 2.6 Å and the structure of an inactive S114A mutant of HsaD   has been determined at resolutions of better than 2 Å with one of several different substrates bound (Lack *et al.*, 2010). It was necessary to use the inactive version of HsaD in order for the substrate/protein complex to be stable enough for crystallisation. In each of the crystal structures, the asymmetric unit consists of two protomers of identical polypeptide chains with one protomer being assigned as the A chain and the other as the B chain. These protomers are identical and each folds to form an α/β hydrolase fold which contains an active site including the catalytic triad (Ser114, His269 and Asp241). (Lack *et al.*, 2008; Lack *et al.*, 2010).

We used a medium throughput platform for screening a well-defined fragment library (Cuilli 2007, 2013) and following subsequent enzyme inhibition studies we identified two fragments namely compound **2** (3,5-dichlorobenzenesulfonamide) and fragment **6** (ethyl 3,5-dichloro-4-hydroxybenzoate), (Table 2) which each have IC_{50} values of less than 1mM. We investigated these compounds and a series of chemical derivatives by both enzymological methods and by determining their crystallographic structures to identify the binding mode. In addition we determined their effects on growth of mycobacteria and *E. coli* for comparison and this is discussed below.

From the series of compounds which we tested, we were able to identify key features of fragment **2** and fragment **6** which were important for inhibition. The important features for inhibition of HsaD by derivatives of **2** appear to be the introduction of a *para* hydroxyl group on the aromatic ring and the presence of two chlorines as *meta* substituents and the inhibitory

potency (IC_{50} of 0.27mM) of fragment **27** supports this conclusion. The potency of derivatives of fragment **6** support the conclusion that the presence of chlorine substituents on the ring at the *meta* positions and the presence of a hydroxyl at the *para* position are important features for inhibition of HsaD.

We obtained the crystal structures of HsaD with compound **2** and a derivative, compound 27, bound. The structure of HsaD with compound **6** could not be determined but we obtained a high resolution structure of HsaD with compound **32** bound. Compound **32** is a derivative of our hit fragment **6**.

Compound **27**, a sulphonate, and compound **32**, a carboxylate, bind to HsaD in a very similar orientation (Fig. 4A) which is distinct from, but overlapping with, the binding site of Compound **2**, an uncharged but polar sulphonamide (Fig. 4B). Specifically, the negatively charged moieties bind in the section of the active site pocket which was identified as the polar sub pocket which accommodates the negatively charged section of each of the negatively charged substrates. including its physiological substrate from cholesterol degradation (Lack et al., 2010).

Whilst each of these inhibitory compounds is bound in the active site, the adjacent nature of these binding sites provides an excellent starting point for growth into new areas of the active site pocket which is a key feature of fragment based drug development (Mancetti et al., 2016.

We have also tested these compounds identified from the screen and their derivatives as inhibitors of growth of *E. coli*, *M. bovis* BCG and *M. tuberculosis*. None of the compounds inhibited growth of *E. coli* at 100 μg/mL (Supplementary Fig 2). In addition, the compounds were found to be non-cytotoxic. Inhibition of growth of both *M. bovis* and *M. tuberculosis* on cholesterol was observed and the potency of inhibition of enzymic activity broadly mirrored the effects on growth. This was the case apart from the potent and negatively charged derivative of compound **2**, namely compound **27**. Its ineffectiveness in the whole-cell inhibition may possibly be due to a lack of permeation through the lipid-rich mycobacterial cell-wall.

We conclude that HsaD is a valid target for antitubercular drug discovery. In view of the growing threat of multi drug resistant tuberculosis no viable target which has characteristics like HsaD should be ignored.

Author Contributions

Elena Polycarpou - carried out experiments, analysed data, co-wrote manuscript Ali Ryan - co-ordinated research, carried out experiments, analysed data, co-wrote article Edith Sim - co-ordinated research as PI, analysed data, wrote manuscript. Dimitrios Evangelopoulos carried out experiments, analysed data, co-wrote manuscript Nathan Lack carried out experiments, analysed data, co-wrote manuscript Romain Ballet carried out experiments, analysed data contributed to manuscript Alice Halman, carried out experiments contributed to manuscript Sanjib Bhakta carried out experiments, analysed data, contributed to manuscript Areej Abuhammad advised on experiments co-wrote manuscript William Jacobs co-ordinated experiments contributed to manuscript Sebastian Keany carried out experiments contributed to manuscript Tim McHugh co-ordinated experiments contributed to manuscript Alessio Ciulli carried out experiments, analysed data co-wrote manuscript. Christian Sieg - carried out experiments, analysed data, contributed to manuscript. Edward Lowe and Olga Eleftheriadou carried out experiments and analysed data.

Competing Interests' Statement

None

References

Adams PD, Afonine PV, Bunkoczi G, Chen VB, Davis IW, Echols N, *et al.* (2010). PHENIX: a comprehensive Python-based system for macromolecular structure solution. *Acta Crystallogr D* **66**(2)**:** 213-221.

Anderton MC, Bhakta S, Besra GS, Jeavons P, Eltis LD, Sim E (2006). Characterization of the putative operon containing arylamine *N*-acetyltransferase (nat) in *Mycobacterium bovis* BCG. *Mol Microbiol* **59**(1)**:** 181-192.

Bardarov S, Bardarov Jr S, Pavelka Jr MS, Sambandamurthy V, Larsen M, Tufariello J*, et al.* (2002). Specialized transduction: an efficient method for generating marked and unmarked targeted gene disruptions in *Mycobacterium tuberculosis*, *M. bovis* BCG and *M. smegmatis*. *Microbiology* **148**(10)**:** 3007-3017.

Bhakta S, Besra GS, Upton AM, Parish T, Sholto-Douglas-Vernon C, Gibson KJ*, et al.* (2004). Arylamine *N*-acetyltransferase is required for synthesis of mycolic acids and complex lipids in *Mycobacterium bovis* BCG and represents a novel drug target. *The Journal of Experimental Medicine* **199**(9)**:** 1191-1199.

Blanco FC, Nunez-Garcia J, García-Pelayo, C; Soria, M, Bianco MV, Zumárraga M, Golby P, Cataldi AA, Gordon SV, Bigi F (2009) Differential transcriptome profiles of attenuated and hypervirulent strains of *Mycobacterium bovis Microbes and Infection* **11**(12); 956-963.

Carr H, Purcell E (1954) Effects of diffusion on free precession in nuclear magnetic resonance experiments. *Phys Rev* **94**:630

Chen VB, Arendall WB, Headd JJ, Keedy DA, Immormino RM, Kapral GJ *et al.* (2010). MolProbity: all-atom structure validation for macromolecular crystallography. *Acta Crystallogr D* 66(1): 12-21

Ciulli A (2013) Biophysical screening for the discovery of small-molecule ligands. *Methods Mol Biol* **1008**: 357-388

Ciulli A, Abell C (2007). Fragment-based approaches to enzyme inhibition. *Curr opin biotechnol* **18**(6)**:** 489-496.

Collaborative Computational Project (1994). The CCP4 suite: programs for protein crystallography. *Acta Crystallogr D* **50**(5)**:** 760-763.

Crowe AM, Stogios PJ, Casabon I, Evdokimova E, Savchenko A, Eltis LD (2015). Structural and functional characterization of a ketosteroid transcriptional regulator of *Mycobacterium tuberculosis*. *J Biol Chem* **290**(2)**:** 872-882.

Curtis MJ, Bond RA, Spina D, Ahluwalia A, Alexander SPA, Giembycz MA et al. (2015). Experimental design and analysis and their reporting: new guidance for publication in BJP. *Br J Pharmacol* 172: 3461–3471

Dalvit C, Pevarello P, Tatò M, Veronesi M, Vulpetti A, Sundström M. (2000) Identification of compounds with binding affinity to proteins via magnetization transfer from bulk water. *J Biomol NMR* 18:65–68.

Dalvit C, Fogliatto G, Stewart A, Veronesi M, Stockman B (2001). WaterLOGSY as a method for primary NMR screening: practical aspects and range of applicability. *J biomol NMR* **21**(4)**:** 349-359.

Emsley P, Lohkamp B, Scott WG, Cowtan K (2010). Features and development of Coot. *Acta Crystallogr D* **66**(4)**:** 486-501.

Evangelopoulos D, Bhakta S (2010). Rapid methods for testing inhibitors of mycobacterial growth. *Antibiotic Resistance Protocols: Second Edition*: 193-201.

Evangelopoulos D, Gupta A, Lack N, Maitra A, ten Bokum AMC, Kendall S L, et al. (2014) Characterisation of a putative *AraC* transcriptional regulator from *Mycobacterium smegmatis*. *Tuberculosis* **94** (6): 664-671.

Evans P (2006). Scaling and assessment of data quality. *Acta Crystallogr D* **62**(Pt 1)**:** 72-82.

Ferguson FM, Fedorov O, Chaikuad A, Philpott M, Muniz JR, Felletar I*, et al.* (2013). Targeting low-druggability bromodomains: fragment based screening and inhibitor design against the BAZ2B bromodomain. *J Med Chem* **56**(24)**:** 10183-10187.

Griffin JE, Gawronski JD, DeJesus MA, Ioerger TR, Akerley BJ, Sassetti CM. (2011) High-resolution phenotypic profiling defines genes essential for Mycobacterial growth and cholesterol catabolism. PLoS Pathog 7(9): e1002251.

Griffin JE, Pandey AK, Gilmore SA, Mizrahi V, McKinney JD, Bertozzi CR, et al. (2012) Cholesterol catabolism by *Mycobacterium tuberculosis* requires transcriptional and metabolic adaptations. *Chem Biol* **19**(2): 218-227.

Hudson SA, McLean KJ, Surade S, Yang YQ, Leys D, Ciulli A*, et al.* (2012). Application of fragment screening and merging to the discovery of inhibitors of the *Mycobacterium tuberculosis* cytochrome P450 CYP121. *Angew Chem Int Ed* **51**(37)**:** 9311-9316.

Hung AW, Silvestre HL, Wen S, George GP, Boland J, Blundell TL*, et al.* (2016). Optimization of Inhibitors of *Mycobacterium tuberculosis* pantothenate synthetase based on group efficiency analysis. *ChemMedChem* **11**(1)**:** 38-42.

Kabsch W (2010). XDS. *Acta Crystallogr Section D* **66**(2)**:** 125-132.

Kendall SL, Burgess P, Balhana R, Withers M, ten Bokum A, Lott JS*, et al.* (2010). Cholesterol utilization in mycobacteria is controlled by two TetR-type transcriptional regulators: kstR and kstR2. *Microbiology* **156**(5)**:** 1362-1371.

Kendall SL, Withers M, Soffair CN, Moreland NJ, Gurcha S, Sidders B*, et al.* (2007). A highly conserved transcriptional repressor controls a large regulon involved in lipid degradation in *Mycobacterium smegmatis* and *Mycobacterium tuberculosis*. *Mol Microbiol* **65**(3)**:** 684-699.

Lack N, Lowe ED, Liu J, Eltis LD, Noble ME, Sim E*, et al.* (2008). Structure of HsaD, a steroid-degrading hydrolase, from *Mycobacterium tuberculosis*. *Acta Crystallogr F* **64**(1)**:** 2-7.

Lack NA, Kawamura A, Fullam E, Laurieri N, Beard S, Russell AJ*, et al.* (2009). Temperature stability of proteins essential for the intracellular survival of *Mycobacterium tuberculosis*. *Biochem J* **418**(2): 369-378.

Lack NA, Yam KC, Lowe ED, Horsman GP, Owen RL, Sim E, *et al.* (2010). Characterization of a carbon-carbon hydrolase from *Mycobacterium tuberculosis* involved in cholesterol metabolism. *J Biol Chem* **285**(1)**:** 434-443.

Li Q, Ge F, Tan Y, Zhang G, Li W, (2016) Genome-wide transcriptome profiling of *Mycobacterium smegmatis* MC^{2}155 cultivated in minimal media supplemented with cholesterol, androstenedione or glycerol *Int J Mol Sci* **17**: 689

Lloyd-Evans E, Lack N, Williams I, Churchill GC, Sim E, Platt FM. (2009) Inhibition of phago-lysosome fusion and foam cell formation by *Mycobacterium bovis* BCG induces a Niemann-Pick type C1 like phenotype. *Chemistry and Physics of Lipids*, **160**: S43–S44.

Lovewell RR, Sassetti CM, VanderVen BC (2016). Chewing the fat: lipid metabolism and homeostasis during *M. tuberculosis* infection. *Current opinion in microbiology* **29:** 30-36.

McCoy AJ, Grosse-Kunstleve RW, Adams PD, Winn MD, Storoni LC, Read RJ (2007). Phaser crystallographic software. *J Appl Crystallogr* **40**(4)**:** 658-674.

McNicholas S, Potterton E, Wilson K, Noble M (2011). Presenting your structures: the CCP4mg molecular-graphics software. *Acta Crystallogr D* **67**(4)**:** 386-394.

Marchetti C, Chan DS, Coyne AG, Abell C (2016) Fragment-based approaches to TB drugs. *Parasitology* DOI: 10.1017/S0031182016001876

Mayer M, Meyer B (1999) Characterization of ligand binding by saturation transfer difference NMR spectroscopy. *Angew Chem Int Ed Engl* **38**:1784–1788.

Mendes V, Blundell TL (2016) Targeting tuberculosis using structure-guided fragment-based drug design. *Drug Discov Today* DOI: 10.1016/j.drudis.2016.10.003

Moriarty NW, Grosse-Kunstleve RW, Adams PD (2009). electronic Ligand Builder and Optimization Workbench (eLBOW): a tool for ligand coordinate and restraint generation. *Acta Crystallogr D* **65**(10)**:** 1074-1080.

Murshudov GN, Vagin AA, Dodson EJ (1997). Refinement of macromolecular structures by the maximum-likelihood method. *Acta Crystallogr D* **53**(3)**:** 240-255.

Niesen FH, Berglund H, Vedadi M (2007). The use of differential scanning fluorimetry to detect ligand interactions that promote protein stability. *Nat Protoc* **2**(9)**:** 2212-2221.

Ouellet H, Johnston JB, Montellano PROd (2011). Cholesterol catabolism as a therapeutic target in *Mycobacterium tuberculosis*. *Trends Microbiol* **19**(11)**:** 530-539.

Pandey AK, Sassetti CM (2008). Mycobacterial persistence requires the utilization of host cholesterol. *Proc Natl Acad Sci U S A* **105**(11)**:** 4376-4380.

Payton M, Gifford C, Schartau P, Hagemeier C, Mushtaq A, Lucas S*, et al.* (2001). Evidence towards the role of arylamine N-acetyltransferase in *Mycobacterium smegmatis* and development of a specific antiserum against the homologous enzyme of *Mycobacterium tuberculosis*. *Microbiology* **147**(12)**:** 3295-3302.

Peyron P, Bordier C, Elsa-Noah N, Maridonneau-Parini I (2000). Nonopsonic phagocytosis of *Mycobacterium kansasii* by human neutrophils depends on cholesterol and is mediated by CR3 associated with glycosylphosphatidylinositol-anchored proteins. *J Immunol* **165**(9)**:** 5186-5191.

Piotto M, Saudek V, Sklenár V (1992) Gradient-tailored excitation for single-quantum NMR spectroscopy of aqueous solutions. *J Biomol NMR* **2**:661–665..

Rebollo-Lopez MJ, Lelièvre J, Alvarez-, Gomez D, Castro-Pichel J, Martínez-Jiménez F, Papadatos G, et al. (2015) Release of 50 new, druglike compounds and their computational target predictions for open source anti-tubercular drug discovery. *PLoS One* **10**(12): e0142293.

Rengarajan J, Bloom BR, Rubin EJ (2005). Genome-wide requirements for *Mycobacterium tuberculosis* adaptation and survival in macrophages. *Proc Natl Acad Sci U S A* **102**(23)**:** 8327-8332.

Rohde K H., Veiga DFT, Caldwell1 S, Bala´ G, Russell DG. (2012) Linking the transcriptional profiles and the physiological states of *Mycobacterium tuberculosis* during an extended intracellular infection. *PLoS Path* **8**(6) e1002769.

Ruzzini AC, Bhowmik S, Ghosh S, Yam KC, Bolin JT, Eltis LD (2013). A Substrate-Assisted Mechanism of Nucleophile Activation in a Ser–His–Asp Containing C–C Bond Hydrolase. *Biochemistry* **52**(42)**:** 7428-7438.

Ruzzini AC, Ghosh S, Horsman GP, Foster LJ, Bolin JT, Eltis LD (2012). Identification of an Acyl-Enzyme Intermediate in a meta-Cleavage Product Hydrolase Reveals the Versatility of the Catalytic Triad. *J Am Chem Soc* **134**(10)**:** 4615-4624.

Ryan A, Keany S, Eleftheriadou O, Ballet R, Cheng H-Y, Sim E (2014). Mechanism-based inhibition of HsaD: a CC bond hydrolase essential for survival of *Mycobacterium tuberculosis* in macrophage. *FEMS microbiology letters* **350**(1)**:** 42-47.

Sassetti CM, Boyd DH, Rubin EJ (2003). Genes required for mycobacterial growth defined by high density mutagenesis. *Mol Microbiol* **48**(1)**:** 77-84.

Silvestre HL, Blundell TL, Abell C, Ciulli A (2013). Integrated biophysical approach to fragment screening and validation for fragment-based lead discovery. *Proc Natl Acad Sci* **110**(32)**:** 12984-12989.

Uhía I, Galán B, Kendall SL, Stoker NG, García JL (2012). Cholesterol metabolism in *Mycobacterium smegmatis*. *Environ microbiol rep* **4**(2)**:** 168-182.

Van der Geize R, Yam K, Heuser T, Wilbrink MH, Hara H, Anderton MC*, et al.* (2007). A gene cluster encoding cholesterol catabolism in a soil actinomycete provides insight into *Mycobacterium tuberculosis* survival in macrophages. *Proc Natl Acad Sci U S A* **104**(6)**:** 1947-1952.

VanderVen BC, Fahey RJ, Lee W, Liu Y, Abramovitch RB, et al. (2015) Novel inhibitors of cholesterol degradation in *Mycobacterium tuberculosis* reveal how the bacterium's metabolism is constrained by the intracellular environment. *PLoS Pathog* **11**(2): e1004679.

Van Molle I, Thomann A, Buckley DL, So EC, Lang S, Crews CM*, et al.* (2012). Dissecting fragment-based lead discovery at the von Hippel-Lindau protein: hypoxia inducible factor 1α protein-protein interface. *Chem biol* **19**(10)**:** 1300-1312.

Westwood I, Bhakta S, Russell AJ, Fullam E, Anderton MC, Kawamura A, Mulvaney A, Vickers RJ, Bhowruth V, Besra GS, Lalvani A, Davies SG, Sim E. (2010) Identification of arylamine N-acetyltransferase inhibitors as an approach towards novel anti-tuberculars. *Protein & Cell* **1**(1) 82-95

Westwood IM, Kawamura A, Russell AJ, Sandy J, Davies SG, Sim E. (2011) Novel small Molecule inhibitors of arylamine N-acetyltransferases: Drug discovery by high throughput screening. *Combinatorial Chemistry & High Throughput Screening* **14**(1): 117-124.

WHO (2015). Global tuberculosis report 2015: http://apps.who.int/iris/bitstream/10665/191102/1/9789241565059_eng.pdf.

Winn MD, Ballard CC, Cowtan KD, Dodson EJ, Emsley P, Evans PR*, et al.* (2011). Overview of the CCP4 suite and current developments. *Acta Crystallogr D* **67**(4)**:** 235-242.

Winter G (2010). xia2: an expert system for macromolecular crystallography data reduction. *J App Crystallogr* **43**(1)**:** 186-190.
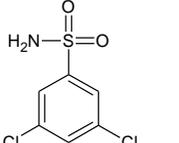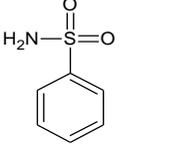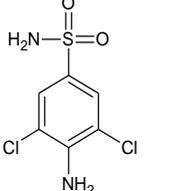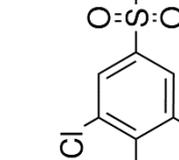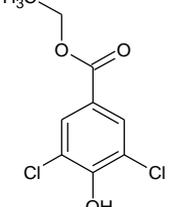
Yam KC, D'Angelo I, Kalscheuer R, Zhu H, Wang JX, Snieckus V*, et al.* (2009). Studies of a ring-cleaving dioxygenase illuminate the role of cholesterol metabolism in the pathogenesis of *Mycobacterium tuberculosis*. *PLoS Pathog* **5**(3)**:** e1000344.

Table 1

Compound	T$_M$ shifts*	NMR	PMSF displacement	Structure
1	1.78; 2.64; 2.64	Hit	Displaced	
2	0.77; 0.38; 0.38	Hit	Displaced	
3	0.55; 0.76; 0.76	Hit	Displaced	
4	0.55; -2.26; -2.26	Hit	Displaced	
5	0.92; 1.13; 1.13	Hit	Not displaced (PMSF bound)	
6	0.70; 1.13; 1.13	Hit	Not displaced (PMSF not bound)	
7	0.82; 0.38; 0.76	Hit	Displaced	
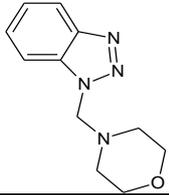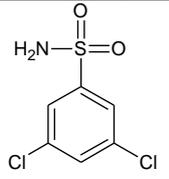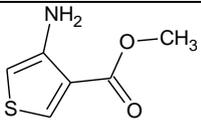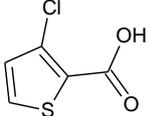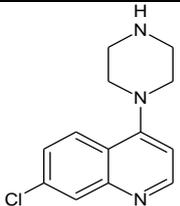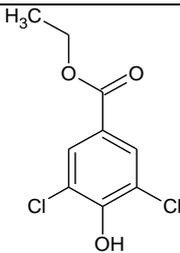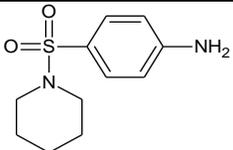
Table 1. Fragments from a 1258 member library producing a significant shift in HsaD T_M. and where saturation NMR demonstrated displacement of the ligand by PMSF.

The compounds are numbered sequentially : 4-((1H-benzo[d][1,2,3] triazol-1-yl)methyl)morpholine compound 1; 3,5,-dichloro-benzenesulfonamide compound 2; methyl 4-aminothiophene-3-carboxylate compound 3; 3-chlorothiophene-2-carboxylic acid , compound 4; 7-chloro-4-(piperazin-1-yl)quinolone, compound 5; ethyl 3,5-dichloro-4-hydroxybenzoate, compound 6; 4-(piperidin-1-ylsulfonyl)aniline, compound 7. *The T_M shifts in °C are shown for each compound tested with a positive result for DSF, performed as described in materials and methods at 2.5 mM final fragment concentration per well. Structures are drawn with ChemDraw Ultra 12.0 (CambridgeSoft). Hits from the primary DSF screen were re-tested twice to confirm results of the initial screen and finally validated for protein binding using NMR spectroscopy (as shown in Fig. 2A) (after Ciulli & Abell, 2007; Mayer & Meyer, 1999).

ID	Compound	Structure	IC$_{50}$ (mM)	MIC (µg/mL) Growth on cholesterol	
				M. bovis BCG	*M. tuberculosis*
2	3,5,-dichloro-benzenesulfonamide		0.41 ±0.02	<12.5	25
8	Benzenesulfonamide		NI	NI	NI
24	3,5-dichlorosulfanilamide		0.16±0.01	25	200
27	3,5-dichloro-4-hydroxybenzenesulphonic acid		0.27 ±0.01	>200	>200
6	ethyl 3,5-dichloro-4-hydroxybenzoate		0.52±0.02	<12.5	<12.5

| **32**	3,5-dichloro-4-hydroxybenzoic acid		0.54 ±0.01	<12.5	200
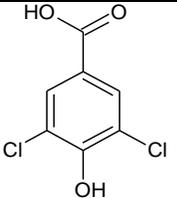
Table 2 Effects of (A)Fragment 2 and its derivatives and (B) fragment 6 and a derivative on HsaD enzymic activity and growth of mycobacteria on cholesterol as carbon source.

NI indicates no inhibition observed at 5mM for inhibition of enzyme activity and no inhibition of growth at 200 μg/mL as described in Methods.

IC_{50} values shown as average ± standard deviation (N=6). See supplementary table 1 for full list.

Table 3 Processing and refinement statistics for X-ray crystallographic structures.

Structure	HsaD - **2**	HsaD - **27**	HsaD - **32**
PDB Code	5JZB	5JZ9	5JZS
Space Group	I $2_1 2_1 2_1$	I $2_1 2_1 2_1$	I $2_1 2_1 2_1$
α, β, γ (°)	90, 90, 90	90, 90, 90	90, 90, 90
a, b, c (Å)	82.03, 82.23, 194.25	81.73, 82.32, 193.58	81.92, 82.27, 195.13
Processing Statistics			
Resolution Range (Å)	50.9-2.1	75.75-2.68	97.57-2.27
Unique reflections [a]	38,700	18,699 (2,445)	30,015 (2,024)
R_{merge}	0.134 (0.469)	0.231 (0.895)	0.109 (0.453)
$<I/\sigma(I)>$ [a]	8 (2.6)	4.4 (1.5)	7.7 (1.4)
Completeness % [a]	100 (100)	99.6 (99.0)	99.3 (57.4)
Multiplicity [a]	6.3 (5.3)	4.4 (4.5)	4.9 (3.1)
Refinement Statistics			
R_{work} %	23.51	24.05	23.48
R_{free} %	20.55	21.27	20.25
RMS bond angle (°)	1.28	0.89	1.20
RMS bond length (Å)	0.005	0.004	0.009
Ramachandran Statistics[b]			
Preferred region %	97.5	98.2	98.6
Allowed region %	2.3	1.8	1.4
Outliers %	0.2	0	0
[a] Numbers in parentheses are for the highest resolution shell.			
[b] Ramachandran statistics were calculated using MolProbity (Chen et al 2010).			
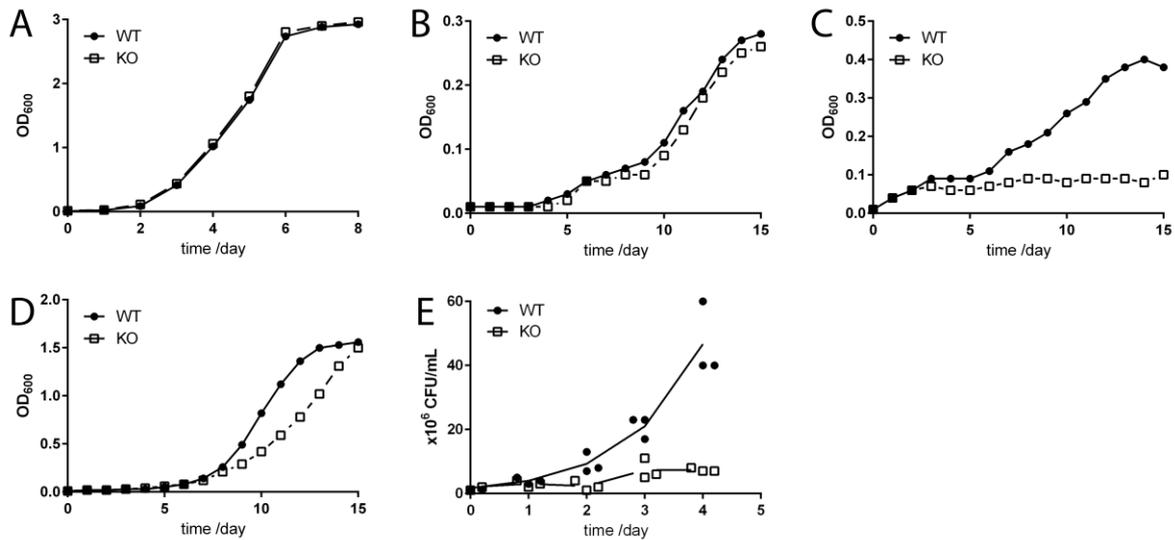
Figure 1. Effect of deletion of *hsaD* gene on *M. bovis* BCG. Growth rates of *ΔhsaD* and wildtype *M. bovis* BCG in MB7H9 (A) on minimal medium containing 0.05% (v/v) tyloxapol, 0.05% (v/v) ethanol with no additional carbon source (B) or supplemented with , 100 μg/mL cholesterol (C) or 100 μg/mL glycerol (D). The symbols show the average values of three independent experiments and the symbols encompass the range of values obtained. The intracellular survival of ΔhsaD *M. bovis* BCG relative to the wild-type in RAW264.7 cells (E) was determined as described in Methods. The results in E are the results of three independent experiments in which the mean values are plotted in a staggered plot. All symbols represent the same sampling time points (days 0,1,2,3,4) but are shown as a cluster for clarity.
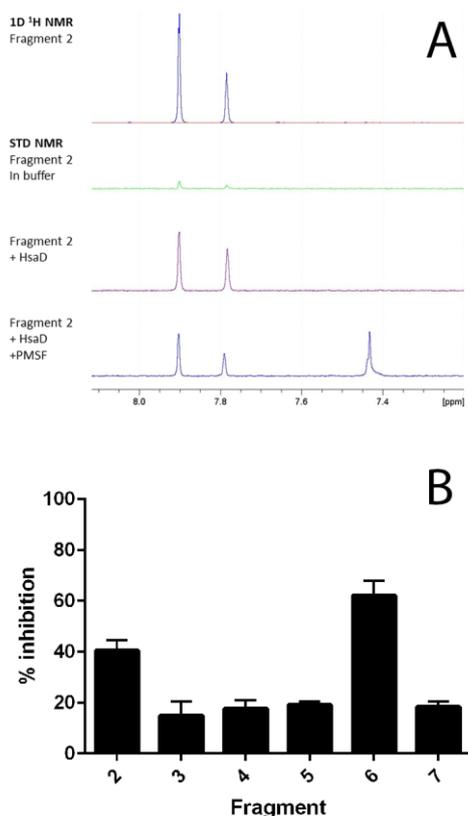
Figure 2A. NMR evidence of fragment binding

Water-suppressed 1D 1H and STN NMR screening spectra for a representative fragment hit (fragment 2, at 1.2 mM) in the presence and absence of HsaD (10 uM) plus PMSF (100 uM). Only the fragment resonances in the aromatic region of the spectra are shown. The strong positive fragment signals in the presence of HsaD (purple spectrum) indicate binding, and this interaction is reduced by the addition of PMSF.

Figure 2 B. Inhibition of HsaD by DSF hits

Fragments identified by DSF as binding to HsaD were assayed for inhibition as described in materials and methods at 1 mM (hollow bars). The mean of 6 independent experiments (each carried out in triplicate) ± standard deviation is shown. Fragments are numbered as shown in Table 1. 100% activity was defined as the rate of enzymatic HOPDA hydrolysis by 16 μg/mL HsaD with vehicle (no compound), which was 0.08 μmol/min/(mg protein).
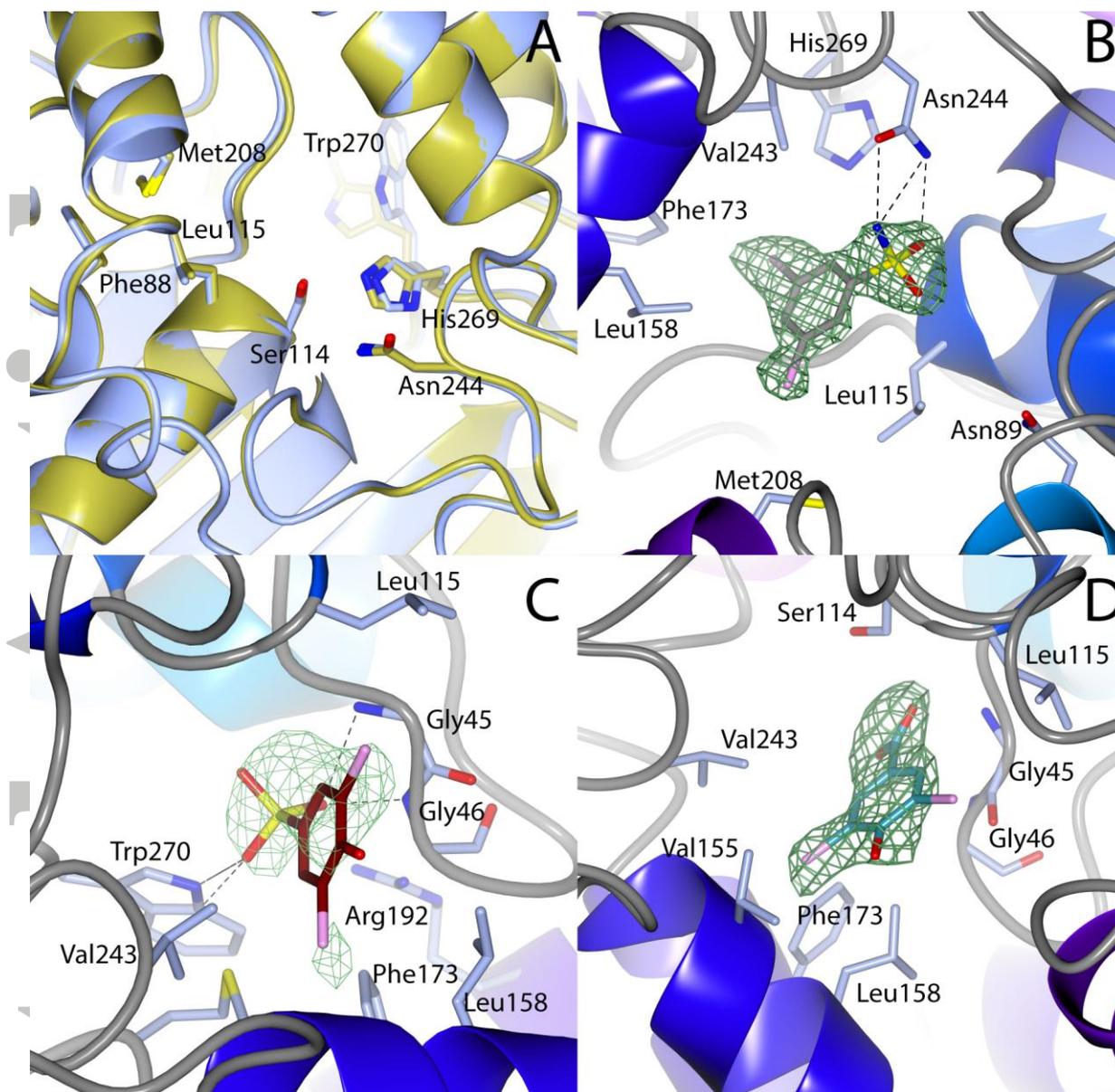
Figure 3. Binding of inhibitors to HsaD. (A) The active site residues of apo HsaD (Lack *et al.*, 2008) are overlaid onto the active site residues of HsaD bound to fragment **27**(fragment not shown). (B) Fragment **2**, (C) Fragment **27** and (D) Fragment **32** each bound to HsaD. In (A) HsaD structure with compound **2** has blue carbon atoms, apo-HsaD has gold carbon atoms. In (B) - (D) Green mesh is unbiased positive difference density contoured at 3σ. In (B) - (D) the protein is shown with blue carbon atoms, **2** is shown with grey carbon atoms, **27** with brown carbon atoms and **32** with cyan carbon atoms. Chlorines are coloured pink and hydrogen bonds are black dashed lines. Interacting residues are labelled. All figures were generated in CCP4MG (McNicholas *et al.*, 2011).
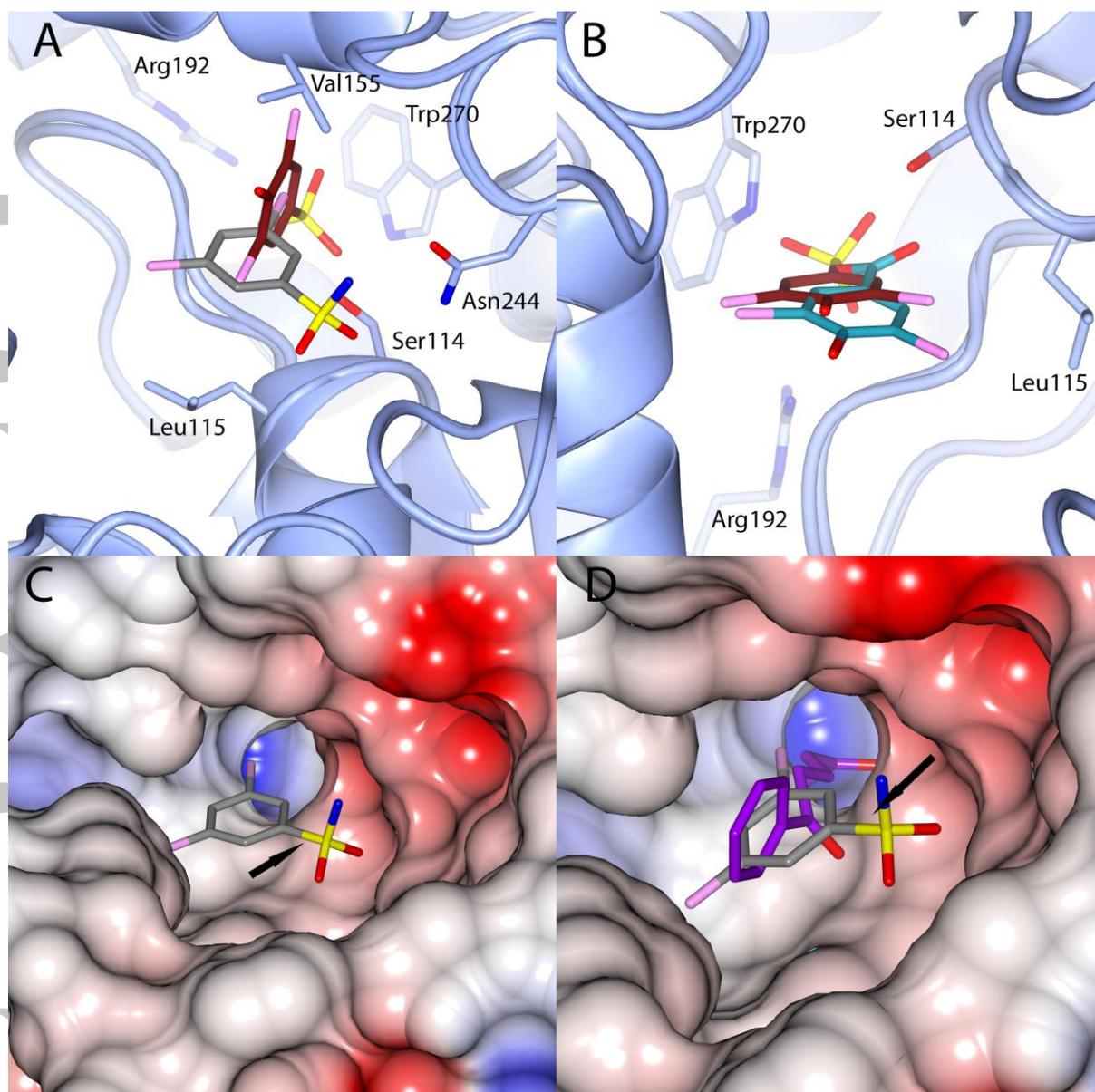
Figure 4. Comparison of the orientation of binding of fragments to the HsaD active site.

(A) Shows the overlaid binding orientations of compounds **27** and **32**. (B) shows the overlaid binding orientations of compounds **2** and **27.** (C) shows the electrostatic potential surface map of HsaD in the pocket around compound **2**. (D) shows an overlay of the structure of HsaD bound to **2** with the structure of HsaD bound to HOPDA (PDB code 2wug) (Lack *et al.*, 2010). Colour coding of carbon atoms is as per figure 3. HOPDA is shown with purple carbon atoms. CCP4MG was used to perform secondary structure alignments for as well as generating the electrostatic potential maps for (C) and (D). In frames A and B the active site Serine residue 114 is shown in stick format. In frames C and D the Serine residue 114 position is indicated by an arrow.